Journal of South American Earth Sciences 96 (2019) 102352

Contents lists available at ScienceDirect

Journal of South American Earth Sciences

journal homepage: www.elsevier.com/locate/jsames

Phanerozoic cooling history of Archean/Paleoproterozoic basement in the southern Espinhaço Range, southeastern Brazil, through apatite fission-track analysis

E. Amaral-Santos[a,*], A.R. Jelinek[a], P.A. Almeida-Abreu[b], F.A. Genezine[c]

[a] Instituto de Geociências, Universidade Federal do Rio Grande do Sul, Brazil
[b] Centro de Estudos em Geociências - ICT, Universidade Federal dos Vales do Jequitinhonha e Mucuri, Brazil
[c] Instituto de Pesquisas Energéticas e Nucleares, Centro do Reator de Pesquisa, Brazil

ARTICLE INFO

Keywords:
Espinhaço Range basement
Quadrilátero Ferrífero
Apatite fission-track thermochronology
Denudation history

ABSTRACT

Apatite fission track thermochronology of basement rocks from the southern Espinhaço Range and Quadrilátero Ferrífero in southeastern Brazil unravels the tectonic history of this portion of the Brazilian Shield. The study area encompasses an Archean and Paleoproterozoic granitoid-gneiss basement, in the southern border of the São Francisco Craton, and an Archean to Paleo-Mesoproterozoic sedimentary cover. Apatite fission track ages (AFT) vary from 187 ± 18 to 91.8 ± 7.3 Ma and horizontal confined track lengths vary from 9.62 ± 1.81 μm to 12.85 ± 1.35 μm. Thermal history modeling shows an accelerated cooling episode starting in the Upper Devonian to Early Permian. After this event, quiescence lasted from 115 to 170 Ma. Apatite samples lack evidence of far-field effects from rifting and opening of the South Atlantic Ocean, and also evidence from alkaline and basaltic magmatism emplacement during Mesozoic-Cenozoic. The AFT thermochronometer remained undisturbed during Transminas mafic dyke swarm intrusion. Finally, the last cooling event in the Espinhaço Range-Quadrilátero Ferrífero basement records ascension to surface temperatures due to epeirogeny after new configurations of the Nazca, South American and African plates. A climatic origin for the ascension is supported by accentuated erosion rates, even though a weathering-prone phase is registered in weathering profiles.

1. Introduction

The Brazilian Shield encompasses several tectonic provinces defined during the Precambrian, particularly the Brasiliano Orogeny during Neoproterozoic and Cambrian, when several cratonic fragments assembled into West Gondwana (De Wit et al., 1988; Trompette, 1994). After this major event, the South American Platform remained bounded to the African counterpart and went through cycles of deposition and erosion (Vasconcelos et al., 1994), until ultimate separation during the Cretaceous. For two decades, assorted attempts to document the thermotectonic evolution of the Brazilian Shield and Atlantic margin were conducted through thermochronology analyses, mainly using the apatite fission track (AFT) method. Gallagher et al. (1994) aimed at unraveling the thermotectonic history of the Brazilian upper crustal segment. Afterwards, many authors (*e.g.* Harman et al., 1998; Carmo, 2005; Cogné et al., 2011, 2012; Japsen et al., 2012; Jelinek et al., 2014) dedicated special attention to the margin as well as to regional transects from hinterland to the coast, relating topography, denudation, and the tectonic controls. These authors also highlighted the opening of the South Atlantic Ocean, alkaline and basaltic magmatism of syn- and post-rifting processes in the AFT record.

The present landscape has high relief surrounded by deeply dissected plains (Spier et al., 2006) in the vicinity of the São Francisco Craton and the Araçuaí-West Congo Orogen border (Fig. 1a). The high relief portion of this major tectonic border encompasses the southern and central Espinhaço Range (SER, CER; Eschwege, 1822) and the Quadrilátero Ferrífero (QF) (Fig. 1a), where denudation patterns were first correlated to geomorphology. Most works emphasized qualitatively the importance of lithology and structures on landscape-shaping processes and developed hypotheses of broad denudation surfaces, such as King (1956) and Abreu (1982). Later, quantitative analyses aimed at further investigating geochemical balance, cooling histories and denudation. Several studies registered denudation through cosmogenic ^{10}Be isotopes (*e.g.*, Salgado et al., 2006, 2007; Cherem et al., 2012; Barreto et al., 2013) — using ^{10}Be isotopes half-life = 1.39 My (Korschinek et al., 2010), weathering profiles associated with ^{40}Ar/^{39}Ar ages (*e.g.*,

* Corresponding author. Instituto de Geociências, Universidade Federal do Rio Grande do Sul, Av. Bento Gonçalves, 9500, Porto Alegre, RS, 91501-970, Brazil.
E-mail address: edgar.amaral@ufrgs.br (E. Amaral-Santos).

https://doi.org/10.1016/j.jsames.2019.102352
Received 12 December 2018; Received in revised form 4 September 2019; Accepted 4 September 2019
Available online 10 September 2019
0895-9811/

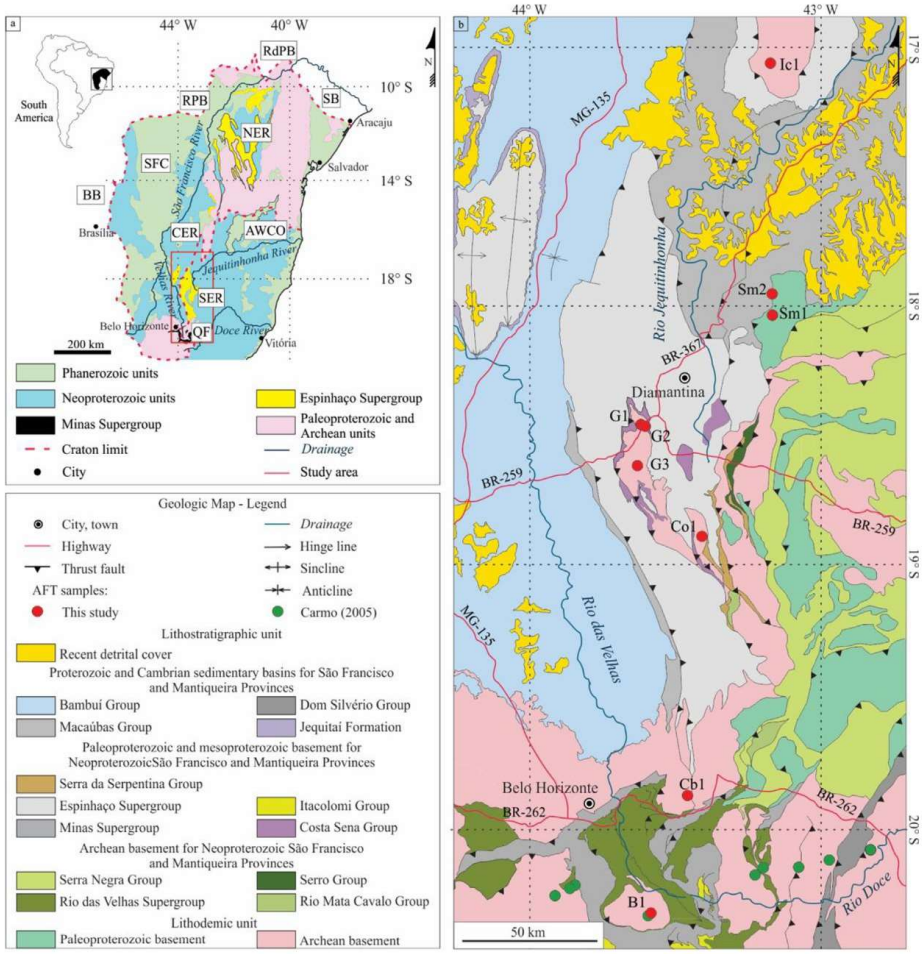

Fig. 1. (a) São Francisco Craton (SFC) location within South America, and adjacent Neoproterozoic mobile belts, Southern Espinhaço Range (SER) and Quadrilátero Ferrífero (QF) province; AWCO: Araçuaí West Congo Orogen, BB: Brasília Belt, RPB: Rio Preto Belt; RdPB: Riacho do Pontal Belt; SB: Sergipano Belt, NER: Northern Espinhaço Range; CER: Central Espinhaço Range. (b) Geological map of the study area with AFT samples analyzed in this study and the Carmo (2005) dataset.

Carmo and Vasconcelos, 2004, 2006; Vasconcelos and Carmo, 2018), and AFT and (U-Th-Sm)/He thermochronology (*e.g.*, Carmo, 2005; Jelinek et al., 2014; Van Ranst et al., 2017).

Progress occurred in constraints of chronology and rates of long-term denudation in the area, but there is still little information on those processes. Because of lack of records in the southeastern Brazilian hinterland, nine AFT samples from the SER and QF province were analyzed to recreate the denudation histories of basement rocks as well as to correlate the cooling and thermal events with vertical displacement of rocks caused by far-field stresses of plate motions. Hence, this study reports the first AFT data quantification of erosion and denudation of this hundred-kilometer scale range, *i.e.*, the Espinhaço Range and QF province. Main results point to two phases of accelerated cooling, with main cause in epeirogenic movements, new plate tectonics rearrangements and slower spreading rates in the mid-Atlantic ridge, interspersed by one phase of slow cooling, interpreted as quiescent tectonism during the Phanerozoic. This modeling also allows an estimate of rock erosion at *ca.* 3300–5000 m since the Upper Devonian.

2. The Brazilian hinterland

2.1. Geological framework

In the Brazilian hinterland, the São Francisco Craton is bounded by the Neoproterozoic Araçuaí, Brasília, Rio Preto, Riacho do Pontal and Sergipano orogenic belts (Almeida et al., 1981, Fig. 1a) that led to assembly of West Gondwana after several collisional events. The basement of the São Francisco Craton has an Archean nucleus and two segments of Paleoproterozoic orogens (Alkmim and Marshak, 1998; Teixeira et al., 2000) that stabilized after the Rhyacian (2.2–2.0 Ga) tectono-metamorphic event (Almeida, 1977). Some of these nucleii outcrop in the Quadrilátero Ferrífero (Alkmim and Martins-Neto, 2012) near the southernmost border of the São Francisco Craton, and along the boundary of the Araçuaí Belt (AWCO, Fig. 1) with the craton. The Espinhaço Range, composed of Proterozoic cover units of the Espinhaço Supergroup, overlies the Archean and Paleoproterozoic basement near the Araçuaí Belt (Fig. 1b).

The southern portion of the N–S trending Archean basement is present in the area. SER and QF are divided into several high-grade granitoid-gneiss complexes whose crystallization ages vary from 3220

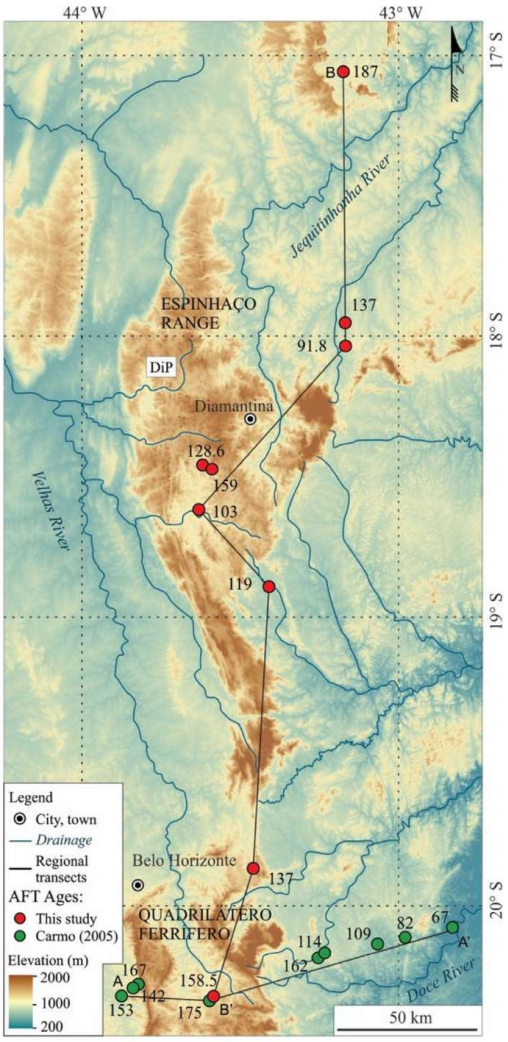

Fig. 2. Geomorphological map of the study area showing both the SER and QF province, AFT age for this study and previous work of Carmo (2005), regional transects (A-A′ and B–B′) and main drainage courses (Doce, Jequitinhonha and Velhas River). DiP: Diamantina Plateau.

to 2680 Ma (Farina et al., 2016). Paleoproterozoic basement is composed of granitoid-gneiss complexes and anorogenic granitoids and was formed between 2.25 and 2.02 Ga (Teixeira et al., 2000; Noce et al., 2000) and 1.75 Ga (magmatic signature of the Statherian Espinhaço rift; Fig. 1b; Chemale Jr. et al., 1998; Fernandes et al., 2000).

The Espinhaço basin of Statherian age records the deposition of rocks that compose the Espinhaço Supergroup, building up the Espinhaço Range, mainly divided into southern and northern segments. Main lithologies are metasandstone, metapelite, metaconglomerate, and lesser metavolcanic and carbonate units, as well as thick banded iron formations bordering the southeastern portion of the SER (Pflug, 1965; Almeida-Abreu, 1995; Dussin and Dussin, 1995; Uhlein et al., 1998, Fig. 2). The Espinhaço Supergroup is divided into the Guinda and Conselheiro Mata Groups. The Guinda Group was defined by Knauer and Ebert, (1997) as a first continental rifting stage and crustal instability, leading to deposition of rocks in continental environments at *ca.* 1.7 Ga. The Conselheiro Mata Group documents tectonic stability through a series of alternating layers of quartzite and phyllite, in general transgressive trend throughout the Espinhaço basin of Stenian to Tonian ages (1.19–0.91 Ga; Dussin and Dussin, 1995; Chemale Jr. et al., 2011). On the other hand, Almeida Abreu and Renger (2002, 2007) considered the Conselheiro Mata Group as deposited in a foredeep basin related to tectonic inversion of the Espinhaço basin by the end of the Mesoproterozoic, $< 906 \pm 2$ Ma (Machado et al., 1989). This is the age of the basaltic rocks of the Pedro Lessa Suite that cut through the tectonic structures of the Espinhaço Supergroup. The hiatus between Guinda and Conselheiro Mata Groups from 1.6 to 1.3 Ga is well documented in the northern portion of the Espinhaço basin (Fig. 1a, northern Espinhaço Range – NER; Chemale Jr. et al., 2011). Records are lacking in the southern area, therefore Chemale Jr. et al. (2011, 2012) interpreted the SER as a structural high or a non-depositional area.

Almeida-Abreu and Renger (2002) favor Mesoproterozoic tectonism for the onset of creation of SER topography, supported by muscovite fission track analyses. Espinhaço Supergroup remained unmetamorphosed after *ca.* 1.1 Ga (Siga Jr. et al., 1987). Muscovite fission track thermochronometry, according to Price and Walker (1963) and Fleischer et al. (1964), records ages > 100 My while fission tracks remained stable at temperatures < 200 °C. On the other hand, Uhlein et al. (1986), Marshak and Alkmim (1989), Trompette et al. (1992) proposed that the Espinhaço Supergroup structures are related to the Brasiliano Orogeny and that the Supergroup remained unaffected by Mesoproterozoic tectonism, based on ductile shear zones and folds with westward vergence.

The Brasiliano event (Almeida, 1977) caused tectonic structuring and inversion of the SER (Uhlein et al., 1986; Dussin and Dussin, 1995; Pedrosa-Soares and Wiedemann-Leonardos, 2000; Pedrosa-Soares et al., 2001), but Almeida-Abreu and Renger (2007) considered this region a glacier dispersion center of the Macaúbas Glaciation at the end of the Mesoproterozoic. Tillites surround the western, northern and northeastern SER, which contains clasts of metasedimentary, granitic and metaultramafic rocks that compose parts of the cordillera. Mountain glaciation, 1.1 and 1.05 Ga in age (D'Agrella Filho et al., 1990), occurred while the SER was an orogenic belt by the end of the Mesoproterozoic. Remnants of glacial valleys (Almeida-Abreu and Renger, 2007) and extensive glacially striated pavements were preserved in the Espinhaço Supergroup (Isotta et al., 1969).

The QF province is composed of supracrustal rocks of Archean to Paleoproterozoic ages deposited on Archean granitoid-gneiss basement (Fig. 1b). The basal unit is the Rio das Velhas Supergroup, a greenstone belt of 2773 Ma (Machado et al., 1992) that hosts world-class gold deposits and a flysch to molasse-type sequence. The Minas Supergroup has maximum age of *ca.* 2.60 Ga (Noce, 1995; Carneiro et al., 1995; Machado et al., 1993, 1996; Hartmann et al., 2006) and unconformably overlies the Rio das Velhas Supergroup as testimony of passive margin basin to a syn-orogenic sedimentary sequence. Finally, the Itacolomi Group (< 2.03 Ga; Hartmann et al., 2006) is separated from the Minas Supergroup by a regional unconformity. This group is interpreted as an intermontane molasse accumulated during the collapse of the Rhyacian orogen (*ca.* 2.095 Ga; Alkmim and Martins-Neto, 2012). The Minas Supergroup together with the Itacolomi Group records a Wilson Cycle between *ca.* 2.5 and 2.0 Ga (Alkmim and Marshak, 1998). The structure of the QF basement is dome-and-keel, in which troughs of Paleoproterozoic supracrustal rocks alternate with domes of Archean basement (Marshak et al., 1997).

2.2. Geomorphologic setting

The study area extends for 300 km from 17 to 20° S in the southeastern border of the São Francisco Craton (Fig. 2), encompassing both SER and QF. The geomorphology in this portion of the Brazilian highlands comprises elevated interior plateaus surrounded by deeply dissected plains that expose Archean and Proterozoic basement (Spier

et al., 2006; Vasconcelos and Carmo, 2018).

Both SER and QF areas have high topographic relief, with elevations reaching 2000 m, such as the Diamantina plateau – DiP (Fig. 2). SER is a residual landscape primarily composed of quartzitic rocks from the Espinhaço Supergroup flanked by less resistant Neoproterozoic Bambuí Group rocks (Paula-Santos et al., 2015, Fig. 1a). As a result, SER most recurrent geomorphologic features refer to scarps, faults, and residual synclines and anticlines responsible for ridges eroded by small streams (Augustin et al., 2014). These streams align with inherited geological lineaments as they deepen channels and expose quartzite outcrops (Fonseca and Augustin, 2014). The major composition of the QF province crests consists of supergene-enriched banded iron formations and quartzite or conglomerate units of the Minas Supergroup and Itacolomi Group. These resistant rocks controlled SER and QF in development of river basins in southeastern-northeastern Brazil: Doce, Jequitinhonha, and São Francisco Rivers (Saadi, 1995; Barreto et al., 2013, Fig. 1a). The study area embodies both Doce and Jequitinhonha Rivers, which flow eastward to the Atlantic Ocean. São Francisco River flows outwards of the study area. However, the largest tributary Velhas River is in central QF, dissecting the Archean and Paleoproterozoic nucleus and the western portion of SER, flowing northward to the São Francisco River. Overall flow is to the north draining the craton into the Atlantic Ocean in northeastern Brazil.

The Diamantina plateau and QF were inspected by the Portuguese during territory recognition in the XVII-XVIII centuries because of deposits of diamond, gold, banded iron formations, manganese, and bauxite (Derby, 2010), some of which are world class (*e.g.*, banded iron formation in QF province). Topographic prominence was also considered significant.

3. Sampling and analytical methods

3.1. Apatite fission-track analysis

AFT study was performed on nine outcrop samples collected in SER and QF. Samples comprise nine igneous rocks of the Precambrian basement, where eight samples were collected in the Espinhaço Range and one sample in the São Francisco Craton. Sampling followed common procedures for AFT analysis, in which bedrock fresh samples from isolated locations were chosen to estimate exhumation and cooling patterns.

To obtain apatite crystals concentrates, samples were ground, sieved, dried at temperatures < 40 °C and submitted to hydraulic and magnetic separation. In sequence, heavy-liquids and hand-picking techniques were performed. Apatite crystals were mounted in epoxy resin, polished to expose internal structure and chemically etched with 5.5 M HNO_3 at 21 °C for 20 s to reveal spontaneous fission tracks. Because of selection of the external detector method (EDM; Hurford, 1990), apatite mounts, U-doped glass dosimeters (CN5) and age standards (Durango) were coupled with low-uranium micas and sent to neutron irradiation in a well-thermalized position in the IEA-R1 research reactor at IPEN, São Paulo, Brazil. Micas were etched for 18 min in 48% HF at 20 °C to reveal induced fission tracks. Samples were dated at the thermochronology facility of Universidade Federal do Rio Grande do Sul. Later, track-count and track-length measurements were conducted at 1000 x (dry) magnification, Leica CTR 6000 microscope paired with Leica Application Suite (LAS) software. AFT ages were calibrated according to the ξ-calibration method (Hurford, 1990), and reported as central ages (Galbraith and Laslett, 1993), gathered through Radial Plotter (Vermeesch, 2009). The fission-track age errors are quoted at the 1σ confidence level. Next, track length distribution analyses (Gleadow et al., 1986) were carried out on lengths measured on horizontal confined fission tracks. Finally, etch pit diameters (Dpar; Donelick et al., 2005) were measured to correlate with apatite composition.

3.2. Thermal history modeling

To understand the thermal history of SER and QF, apatite thermal history modeling was performed using HeFTy 1.8.0. software (Ketcham, 2005) based on the annealing model of Ketcham et al. (2007), with Dpar values as a kinetic parameter. Inversions were run with 200,000 randomly chosen time-temperature histories for each sample, in a way that enough model paths were available to differentiate "good fit" from "acceptable fit" (see Ketcham et al., 2000 for details and definitions of "good" and "acceptable" fits). Restricted conditions were imposed on each inversion modeling, grouped in two different sets. Group 1: (a) initial t-T box constraint set at the base of the apatite partial annealing zone at 120 °C until 200 °C, and time between 400 and 300 Ma, which corresponds to the oldest grain ages or somewhat older than the oldest ages of a sample; (b) the present-day mean surface temperature was set at 20 ± 10 °C. Group 2: (a) initial t-T box constraint analogous to Group 1; (b) t-T box constraint set between 250 and 120 Ma and temperature at 50 ± 30 °C to simulate lower temperatures; (c) t-T box constraint between 130 and 110 Ma and temperature at 90 ± 30 °C corresponding to rifting, to model non-monotonic behavior; (d) a box constraint from 80 to 50 Ma and temperature at 90 ± 30 °C to simulate heating of post-rifting magmatism; (e) the present-day mean surface temperature set at 20 ± 10 °C.

4. Results

4.1. Apatite fission-track data

AFT analytical data from new and available Archean and Paleoproterozoic basement samples are presented in Table 1 and apparent central ages in Fig. 2. We dated 20 grains and measured 100 horizontal confined track lengths per sample. Samples that failed these criteria (Table 1) were retained, because their ages and mean track length (MTL) broadly agree with the nearby samples with good-quality measurements. In general, the new AFT ages range from 187 ± 18 Ma to 91.8 ± 7.3 Ma with mean confined tracks varying from 9.62 ± 1.81 μm to 12.85 ± 1.35 μm and presenting unimodal distribution (Fig. 3 and Fig. 4). Dpar values range from 1.251 to 1.597 μm. Dpar is not a proxy for Cl wt.%, but correlates positively with Cl, and Dpar values are smaller than 1.75 μm; this indicates that apatites have smaller resistance to annealing (Donelick et al., 2005).

Published AFT thermochronological data are not available in the study area. However, Carmo (2005) investigated the subject in the QF and in the Brazilian plateau. The geochronology of weathering during the Cenozoic in southeastern Brazil provided nine AFT ages from 175 ± 7 to 67 ± 4 Ma (Table 1 and Fig. 2). Horizontal confined track lengths vary from 9.99 ± 1.2 to 13.4 ± 0.2 μm (Table 1).

All apatite central ages are younger than their stratigraphic Archean and Paleoproterozoic ages, suggestive of cooling at temperatures lower than Phanerozoic 120-60 °C isotherms. These ages are also younger than the Brasiliano/Pan-African orogeny that affected the São Francisco Craton and adjacent areas until 560 Ma (Brito Neves et al., 2014), leading to the interpretation that such ages are evidence of cooling ages that represent regional denudation events. All central AFT ages (Table 1) passed in χ^2 test pointing to a single population (Galbraith, 1981, Fig. 5). Samples were collected at elevations higher than 700 m in a mountainous area, but the AFT dataset lacks evidence of correlation between AFT apparent ages and elevation (Fig. 6a, A-A′ regional transect). The Carmo (2005) dataset has strong correlation between AFT apparent ages and altitude (Fig. 6b, B–B' regional transect), because samples followed a W-E oriented profile across the QF. Similar positive correlation exists for the complete data set (Fig. 6c).

4.2. Thermal history modeling

To further constrain the thermal and denudation history of SER and

Table 1
New and available apatite fission track data from the Southern Espinhaço Range and Quadrilátero Ferrífero province, southeastern Brazil.

Sample	Lithology	Easting	Northing	Elevation (m)	N	ρs (Ns) ($x10^5$)	ρi (Ni) ($x10^5$)	ρd (Nd) ($x10^5$)	P ($\chi 2$) (%)	U Content (ppm)	Age ± 1σ (Ma)	n	MTL (μm)	Std. Dev. (μm)	Dpar (μm)
B1	Granite	636,202,20	7,752,192,55	958	20	19.2 (578)	15.2 (458)	8.05 (16,105)	74	24	158.5 ± 9.9	100	12,80	1,09	1,43
Cb1	Gneiss	651,682,00	7,802,144,00	1050	20	28.4 (550)	26 (505)	8.05 (16,105)	42	41,1	137.0 ± 8.4	100	12,83	1,20	1,43
Co1	Rhyolite	657,831,66	7,911,755,16	667	13	8.92 (290)	10.8 (352)	8.05 (16,105)	0	17,1	119.0 ± 18	10	12,49	1,90	1,60
G1	Gneiss	632,104,25	7,959,090,15	1044	20	22.6 (576)	22.1 (564)	8.05 (16,105)	93	34,9	128.6 ± 7.6	100	12,85	1,35	1,38
G2	Gneiss	633,780,70	7,958,401,87	1023	20	14.5 (420)	11.4 (330)	8.05 (16,105)	40	17,9	159.0 ± 13	64	12,75	1,27	1,42
G3	Granite	630,495,33	7,941,650,19	967	8	5.28 (67)	6.54 (83)	8.05 (16,105)	56	10,3	103.0 ± 14	–	–	–	–
Ic1	Granite	686,811,45	8,112,105,79	777	20	11.2 (267)	7.49 (169)	8.05 (16,105)	100	11,8	187.0 ± 18	14	12,04	2,13	1,59
Sm1	Granite	687,666,71	8,005,384,01	716	20	12.2 (274)	16.8 (377)	8.05 (16,105)	96	26,5	91.8 ± 7.3	22	11,60	1,73	1,25
Sm2	Granite	687,654,90	8,014,389,45	411	20	12.9 (474)	11.9 (475)	8.05 (16,105)	29	18,7	137.0 ± 10	21	9,62	1,81	1,25
FTSEB-20*	Gneiss	599,997,91	7,752,307,43	800	20	9.701 (470)	11.81 (572)	9.80 (4183)	98	15	153.0 ± 10	100	11,50	0,30	3,00
FTSEB-21*	Granite	607,044,52	7,755,552,31	1030	23	3.443 (327)	4.58 (435)	9.94 (4183)	95	6	142.0 ± 11	100	11,70	0,30	2,80
FTSEB-22*	Granite	608,657,92	7,756,383,41	1160	26	3.596 (287)	4.11 (328)	10.09 (4183)	56	5	167.0 ± 14	100	11,70	0,20	2,20
FTSEB-24*	Gneiss	636,529,34	7,752,078,65	960	20	13.16 (1465)	14.83 (1651)	10.38 (4183)	52	18	175.0 ± 7	100	11,70	0,30	3,10
FTSEB-29*	Granite-Gneiss	677,606,96	7,751,703,92	680	6	11.16 (200)	13.73 (246)	10.53 (4183)	24	16	162.0 ± 16	30	11,70	0,30	1,60
FTSEB-30*	Quartzite	681,083,03	7,772,515,12	680	28	1.752 (169)	3.11 (300)	10.67 (4183)	28	4	114.0 ± 11	13	11,70	1,20	4,40
FTSEB-31*	Gneiss	686,862,07	7,773,649,72	590	20	14.99 (1174)	28.25 (2211)	10.82 (4183)	65	33	109.0 ± 5	100	11,70	0,30	2,80
FTSEB-32*	Gneiss	712,748,26	7,775,124,19	700	20	10.11 (998)	24.19 (2389)	10.97 (4183)	50	28	87.0 ± 4	100	11,70	0,30	2,60
FTSEB-34*	Gneiss	732,160,46	7,781,210,82	240	26	2.827 (432)	8.96 (1370)	11.11 (4183)	93	10	67.0 ± 4	100	11,70	0,20	1,60

N: number of apatite crystals analyzed to determine track densities; ρs: measured spontaneous track density; Ns: number of spontaneous tracks counted; ρi: measured induced track density; Ni: number of induced tracks counted; ρd: track density measured in external detector adjacent to glass dosimeter during irradiation; Nd: number of tracks counted in determining ρd; P ($\chi 2$): chi-squared probability; n: number of confined tracks length measured; - no horizontal confined track length measured; Coordinates in UTM, Datum WGS84.

Apatite ages calculated using a zeta of 315.7899 for CN5 glass on Brazil reator. Analyst: E. Amaral Santos.

*Apatite ages calculated using a zeta of 384 ± 5 for Australian Lucas Heights Research Facility (HIFAR) reactor. Analyst: A. Raza.

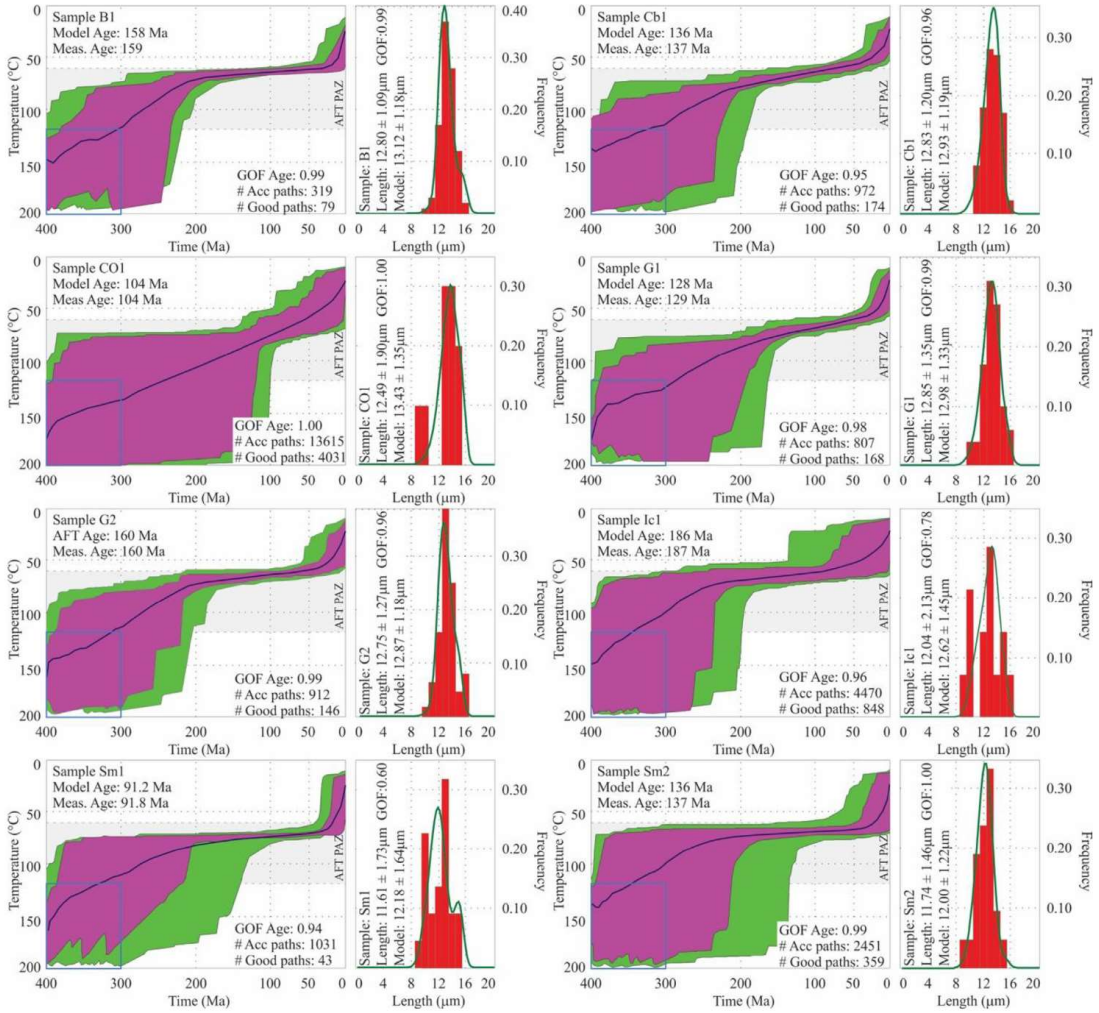

Fig. 3. AFT thermal history models and related mean track length (MTL) distribution for Group 1 samples. In the thermal history models, the green shading represents acceptable paths, magenta shading indicates good paths, the dark blue line is the weighted mean path whereas the light blue box in the bottom left corner of each thermal history is the t-T box constraint used. Comparison of modeled ages and measured ages are shown in the left upper corner. AFT PAZ: Apatite Fission Track Partial Annealing Zone. MTL distribution placed next to the thermal history models are represented as red bars. The green line points to the track lengths modeled. Comparison of model lengths and measured lengths are shown. GOF: Goof of Fit. (For interpretation of the references to colour in this figure legend, the reader is referred to the Web version of this article.)

QF, inverse t-T histories were modeled for eight samples; four had sufficient confined tracks to perform good-quality measurements and four had poor tracks. However, the set with poor tracks was retained because its AFT ages agree with nearby samples whose thermal histories rely on good-quality data. The models constructed, divided into Groups 1 and 2, are shown in Figs. 3 and 4. Fig. 3 presents the thermal histories of eight samples whereas Fig. 4 shows the histories of four samples with better constrained data. There is no clear relationship between AFT ages and track length measurements. As a result, complex t-T histories were expected when the AFT dataset was analyzed (Gallagher et al., 1998).

In modeling histories shown in Fig. 3, the samples started to cool at a range of times, from 340 to 280 Ma. This accelerated cooling event brought samples up from temperatures above the AFT PAZ to the 70 °C limit. Samples had similar trends while cooling, reaching the end of this first cooling episode between 235 and 155 Ma. After cooling to this point, the samples were at temperature near ~70 °C and stayed tectonically quiescent up to approximately 135 Ma. Such dormant activity lasted from 175 Ma (sample Sm1 and Sm2) to 105 Ma (sample Ic1) and started in the Middle Triassic-Lower Jurassic until the Eocene-Oligocene. All samples show accelerated final cooling to surface temperature in the last 20 Ma. Sample Co1 presents monotonic t-T cooling history that began later than all samples at 250 Ma, where the sample cooled from temperature well above the AFT PAZ until reaching present day surface temperature. Such monotonic history interpretation was caused by poorly constrained track-length measurements (Table 1), not fully representative of a t-T history, although its AFT age correlates to the neighboring samples.

As for the thermal histories of Fig. 4 and considering the weighted mean path, the onset of cooling ranges from 280 to 200 Ma. The first

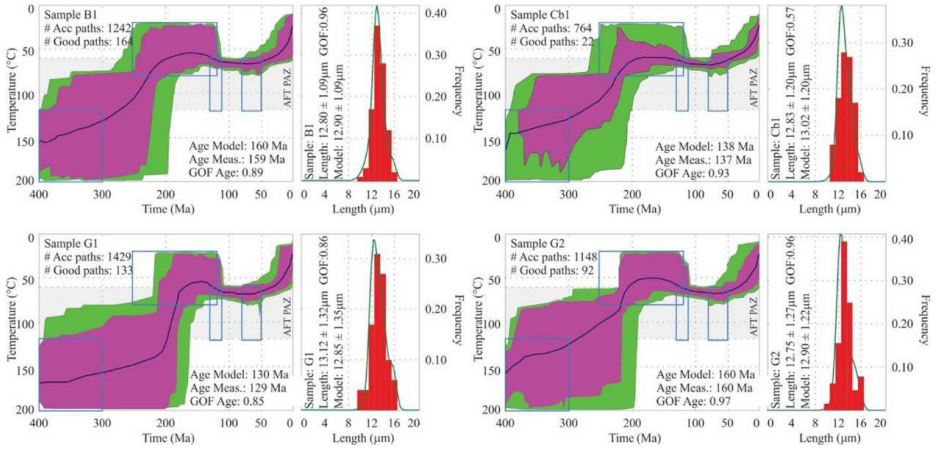

Fig. 4. AFT thermal history models and related mean track length (MTL) distribution for Group 2 samples. In the thermal models, the green shading represents acceptable paths, magenta shading indicates good paths, the dark blue line is the weighted mean path whereas the light blue boxes of each thermal history are t-T constraints. Comparison of modeled ages and measured ages are shown at the right bottom corner. AFT PAZ: Apatite Fission Track Partial Annealing Zone. The MTL distribution placed next to the thermal history models are represented as red bars. The green line represents the modeled track lengths. Comparison of the model lengths and measured lengths are shown. GOF: Good of Fit. (For interpretation of the references to colour in this figure legend, the reader is referred to the Web version of this article.)

accelerated cooling event, initiated at temperature in excess of 120 °C, cooled samples to temperatures of *ca.* 60-50 °C. After cooling, samples registered reheating of *ca.* 10 °C, from 200 to 150 Ma until 80-60 Ma, or 60–70 °C if considering the better paths generated in the thermal histories. Finally, all four samples register accelerated cooling to surface temperature initiated at *ca.* 80-60 Ma.

5. Discussion and interpretation

AFT modeling indicates that SER and QF were characterized in the Phanerozoic by two rapid cooling events interspersed either with an event of slow exhumation rate or a reheating event, according to models of Groups 1 and 2. The AFT apparent ages of the samples collected for this study range from 187 to 91.8 Ma. These ages lack correspondence with the rifting processes that caused West Gondwana breakup into South America and Africa at *ca.* 130 Ma (Chang et al., 1992). A diffuse relationship between AFT ages and MTL is suggestive of AFT ages associated with relatively shortened mean track lengths ($11 \leq MTL \leq 13\,\mu m$) – *i.e.*, samples resided in the AFT PAZ for a long time, supporting the assumption of AFT apparent ages lacking particular correspondence to rifting. Considering both set of models, this claim supports the first group of thermal models. The second set, however, displays reheating associated to the effects of increased heating in a rifting context, reducing lengths by thermal annealing, as well as longer fission tracks generated after reheating. As a result, we expect either a bimodal distribution related to partial annealing or one sharp peak in the MTL chart next to the thermal models, in the case of complete annealing (Green, 1986). Since the measured lengths lack this information, this brings the first evidence to reject the second set of models. The AFT dataset indicates that the fission tracks of all samples were annealed for ages older than Upper Devonian. This raises the hypothesis that the samples resided in crustal levels at temperature in excess of 120 °C before the Devonian. Muscovite fission track age of 1180 ± 90 Ma provided by Siga Jr. et al. (1989) suggests that the muscovite crystal went through the 200–250 °C temperature window during the Mesoproterozoic and that the Brasiliano orogeny (560 Ma; Brito Neves et al., 2014) did not contribute to increase the temperature to further affect crystal stability.

Present-day geothermal gradient in the São Francisco Craton and its sedimentary intracratonic basin varies from 14 to 42 °C.Km^{-1} (Alexandrino and Hamza, 2008) and from 25 to 30 °C.Km^{-1} in the AWCO domain (Schannor, 2018). Few measurements are available to assess the spatial variation of the geothermal gradient that encompasses the area of this study. Therefore, values of 20, 25 and 30 °C.Km^{-1} are assumed, to estimate a range of denudation rates and erosion (Tables 2a and 2b), even though the geothermal gradient is considered constant through time to further build the thermal history of each sample. These values were chosen since they best represent the present-day geothermal gradient in the region and most of the geothermal gradients in the Earth's crust (Burbank and Anderson, 2001). The low-temperature thermal history of rocks in a cratonic environment and borders is mainly controlled by their vertical displacement relative to Earth's surface. Therefore, denudation is the major controlling process in this context (Gallagher et al., 1994, 1995).

For the first cooling episode of samples from Group 1 (Fig. 3), evidenced by the inversion modeling of AFT ages, mean track lengths and Dpar, the samples entered in the PAZ during the Upper Devonian-Early Permian and reached the upper limit during the Middle Triassic-Lower Jurassic, an event that lasted 135 Ma. Rates of denudation (Table 2a) from the analyses of individual t-T history paths vary from 7.6 (sample Sm1) to 21.7 m.Ma^{-1} (sample B1, G1 and G2) while the amount of rock denudation (Table 2b) at this time varied from 1333 m (sample Sm1) to 2500 m (samples B1, G1, G2, Sm2).

Taking Group 1 into account, according to Potter (1997), during the Permian to Early Cretaceous, the South American platform and neighboring African terranes were exposed to weathering and erosion. For King (1956), the SER region developed upwarping from the mid-Paleozoic and this region fully developed Gondwana and post-Gondwana erosion surfaces. The former surface has today few remnants visible at high altitudes in the referred mountain range and in the QF, probably eroded by the younger planation surfaces, such as the Sul-Americana. As a result of the topographic prominence of the SER occupying an upwarped region caused by epeirogenic movements of low amplitude and long wavelengths, São Francisco River occupies the low plain west of this range (Fig. 1a). Potter (1997) established the age of São Francisco River as post-Early Cretaceous, since no large rivers were present earlier in the Brazilian plateau due to aridity (Petri and Campanha, 1981). Our thermochronological data suggest that since the Devonian-

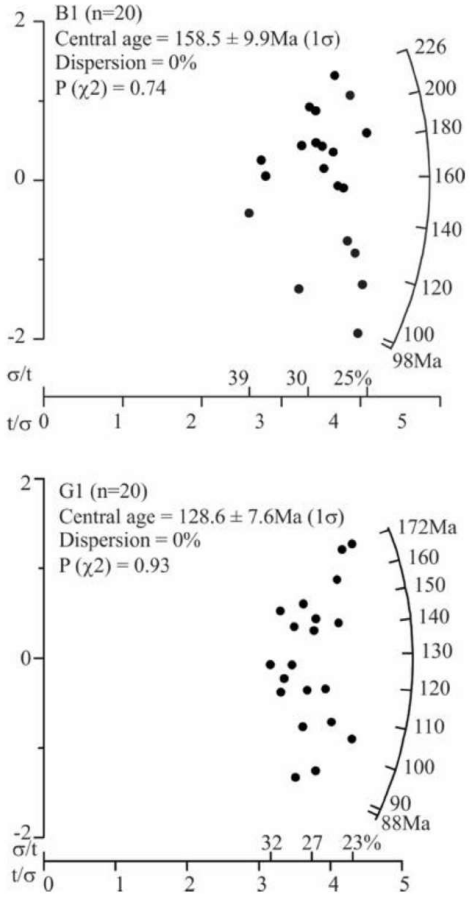

Fig. 5. Two representative samples of QF province (Sample B1) and SER (Sample G1) plotted on Radial Plotter (Vermeesch, 2009) exhibiting their central age and pointing to one single population (Galbraith, 1981).

Permian until the Middle Triassic-Lower Jurassic there was active exhumation taking place in the southern border of the São Francisco Craton and that epeirogeny caused by the Gondwanide orogeny (Permo-Triassic in age; Trouw and De Wit, 1999) was the cause. Jelinek et al. (2014) tentatively extended this proposition to samples of the Sertaneja Depression, in a cratonic environment in northeastern Brazil.

When analyzing the minor cooling registered in the models of Group 1, most samples were already in a slow exhumation phase at *ca.* 180 Ma. This led to model Group 2 samples. The result of this modeling, only performed on samples with statistical robustness, provides good thermal histories for most of the samples and indicates that they were in near-surface temperature before rifting, since *ca.* 180 Ma. Modeling allows for 10–60 °C of reheating, potentially associated with rifting during West Gondwana breakup. However, we favor the monotonic cooling event, based on moderate amount of heating and range of temperatures of 20–70 °C, in which there is only limited sensitivity of the AFT method.

From the Middle Triassic-Lower Jurassic to Eocene-Oligocene, while tectonically quiescent, B1 and Cb1 samples register the lowest and highest denudation rates and amounts of erosion from 2.0 to 6.7 m.Ma^{-1} for denudation and from 333 to 1000 m of rock section removed (Tables 2a and 2b). Slow exhumation rates were the new condition during this phase due to dormant behavior of Earth's crust in this region. Samples belonging to Group 2 show reheating in this scenario, which contrasts with slow exhumation in Group 1. Increase in basal heat flow compensates cooling in a rifting setting, which explains slow exhumation observed in Group 1. However, considering the constraints of Group 2 models that support heating, observed paths are localized near the colder limit of the t-T box. This localization is interpreted as consequence of box constraining the runs to follow colder paths; non-monotonic thermal history is more appropriate. We disfavor the non-monotonic cooling scenario (Group 2) in place of the monotonic histories (Group 1) because of some fundamental factors: (1) lack of sharp peak or bimodality in the MTL chart; (2) forced heating in the models; (3) lack of geological evidence to support the lower temperature box constraint; (4) presence of reheating near the AFT PAZ upper limit. The AFT method registers thermal histories of samples in temperature between 60 and 120 °C, so we cannot assume the existence of events not encompassed by this temperature window or at the threshold of the detection method.

In this quiescent phase, while rifting was happening at the plate boundary between the South American and African plates, samples residing in the continental interior remained unstressed by the forces causing break-up. This is counterintuitive, but the exposed basement of the cratonic regions in Brazil do not record heating caused by rifting stages of the South Atlantic breakup, as evidenced by Harman et al. (1998), Jelinek et al. (2014) and Engelmann de Oliveira and Jelinek (2017). In the São Francisco Craton, the Mata da Corda Group records a manifestation of South Atlantic opening in a series of volcanic deposits (Sgarbi et al., 2001; Mohriak and Leroy, 2012), even though magmatism of this group did not affect the rocks of this study. This rifting process, responsible for the opening of the South Atlantic Ocean, started as early as Late Jurassic (< 150 Ma; Kuchle et al., 2011) in northeastern Brazil for the southern and central branches of the Atlantic rift system, whereas in southeastern Brazil the rifting process occurred mainly between 127 and 113 Ma (Chang et al., 1992). The t-T history modeling has no disturbance caused by basalt magmatism of the Paraná-Etendeka Large Igneous Province (PELIP) that formed when break-up was taking place at the plate boundaries in the Lower Cretaceous (135–125 Ma; Rocha-Campos et al., 1988). No evidence is related to the alkaline rock emplacement in the Late Cretaceous-Paleogene (80-50 Ma) in southeastern Brazil (Almeida et al., 1996; Moreira et al., 2006). In samples from the São Francisco Craton in the Sertaneja Depression, northeastern Brazil, Jelinek et al., (2014) saw no evidence of thermal and tectonic processes related to continental rifting. Lack of magmatism during prerifting and rifting events (Chang et al., 1992) in northeastern Brazil supports the observation. Additional support of quiescence in QF was provided by Spier et al. (2006) and Vasconcelos and Carmo (2018); from 70 to 40 Ma, active weathering and slow erosion took place, indicated by alternating periods of weathering-prone and erosion-prone intervals (Vasconcelos et al., 1994).

The Transminas mafic dyke swarm of Mesozoic age (Dussin, 1994; Chaves and Neves, 2005b; Chaves, 2013) in the southeastern Espinhaço Range is correlated to initial stages of West Gondwana breakup. Thermal and tectonic disturbance in the area is absent in the samples analyzed. After introducing heating correlated to the Transminas mafic dyke swarm in the models, we point out that the models provided few good thermal histories similar to construction without the heating constraint, leading us to discard them. Also, we introduced heating constraint boxes in the models correlated to South Atlantic opening (130–110 Ma) and post-rifting magmatic emplacement (80–50 Ma). Basement rocks of both SER and QF stayed undisturbed by basaltic and alkaline magmatism because of absence of thermal history in the models.

Thermal histories performed by Carmo (2005) in the QF suggest slow cooling from ~80 to 90 °C to the surface and evidence of variable ages for the onset of cooling. Carmo (2005) used a geothermal gradient of 35 °C.km^{-1} and estimated rock denudation of 2–1.7 km for the QF. However, data were modeled in the Monte Trax – v.2 Software

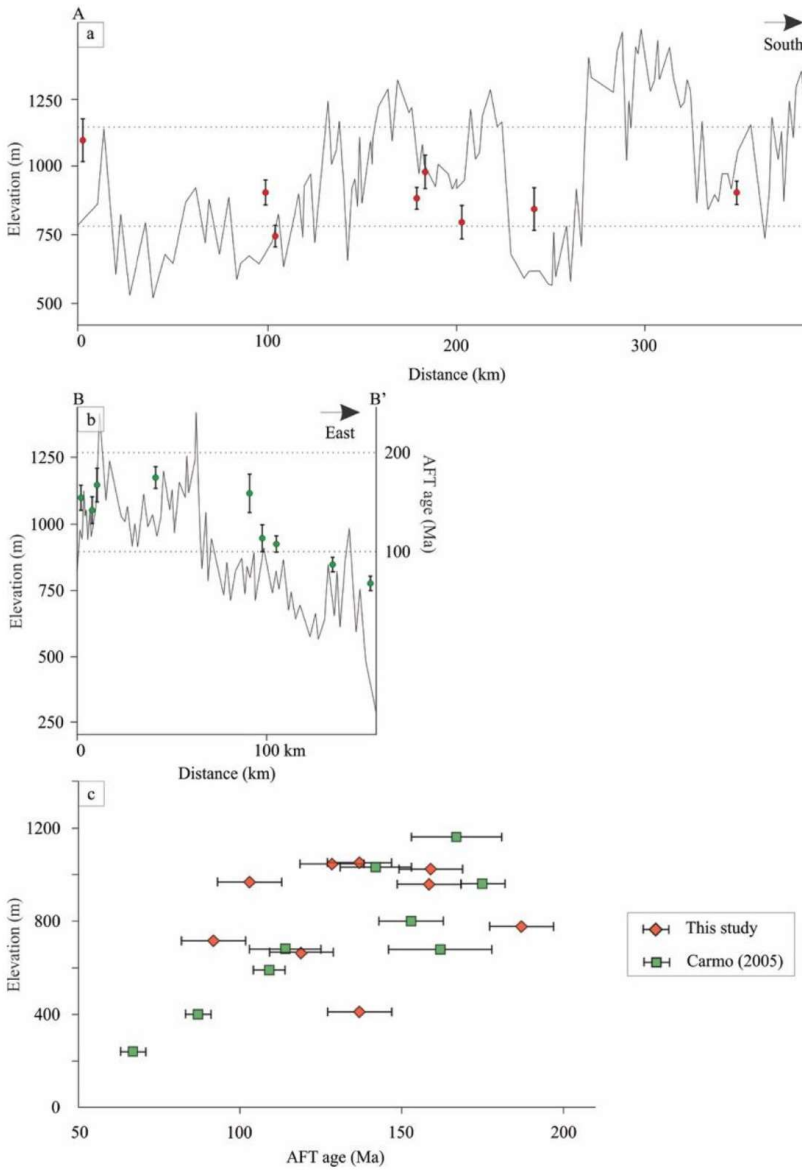

Fig. 6. Regional topographic transects showing elevation and AFT ages, (a) A-A′ transect for this study; (b) B–B′ transect for Carmo (2005) dataset. (c) Altitude vs. AFT age chart including Carmo (2005) dataset.

(Gallagher, 1995) without incorporating the annealing model of Ketcham et al. (2007) used in this study. This last model sheds light and updates the understanding of kinetics of annealing of apatite regarding the reproducibility of track length measurements.

Van Ranst et al. (2017) provided AFT ages ranging from 90.1 to 49.7 Ma for the AWCO domain that agree with ages found by Jelinek et al. (2014) and Carmo (2005) for the same region, which may be related to reactivation of inherited structures during the post-rifting phase of the South Atlantic opening. Jelinek et al. (2014) also contributed with AFT ages for the AWCO domain whose modeled histories showed accelerated cooling through the PAZ between 140 and 80 Ma, contrasting with quiescent tectonism in the western border of this domain, in the SER.

All samples in this study show recent cooling since Eocene-Oligocene from temperature of 50–70 °C to surface conditions at 20 °C. This cooling may be an artifact caused by numerical inversion of track-length data, even though they are reproducible, predicted and designed to reduce “recent-cooling” after using Ketcham et al. (2007) annealing model. Furthermore, because this cooling phase started at temperature close to the upper limit where fission tracks are partially annealed, regional events encompassing all samples must provide enough support for further discussions. Many authors (Gallagher et al., 1994, 1995; Harman et al., 1998; Carmo, 2005; Hiruma et al., 2010; Cogné et al., 2011, 2012; Japsen et al., 2012; Jelinek et al., 2014; Engelmann de

Table 2
(a) Denudation rates and (b) Amount of erosion for each cooling episode, considering the geothermal gradients of 20, 25 and 30 °C.Km^{-1}.

a)	Cooling Episode 1			Quiescent phase			Cooling Episode 2		
Samples	Denudation Rates (m.Ma^{-1})			Denudation Rates (m.Ma^{-1})			Denudation Rates (m.Ma^{-1})		
B1	21,7	17,4	14,5	2,9	2,4	2,0	80,0	64,0	53,3
Cb1	14,5	11,6	9,7	6,7	5,3	4,4	87,5	70,0	58,3
G1	21,7	17,4	14,5	3,6	2,9	2,4	80,0	64,0	53,3
G2	21,7	17,4	14,5	3,0	2,4	2,0	57,1	45,7	38,1
Ic1	21,4	17,1	14,3	5,0	4,0	3,3	23,5	18,8	15,7
Sm1	11,4	9,1	7,6	6,5	5,2	4,3	56,3	45,0	37,5
Sm2	14,3	11,4	9,5	3,6	2,9	2,4	80,0	64,0	53,3
CO1	24,0	19,2	16,0	–	–	–	–	–	–
Geothermal Gradient (°C.Km^{-1})	20	25	30	20	25	30	20	25	30
b) Samples	Cooling Episode 1 Erosion (m)			Quiescent phase Erosion (m)			Cooling Episode 2 Erosion (m)		
B1	2500	2000	1667	500	400	333	2000	1600	1333
Cb1	2250	1800	1500	1000	800	667	1750	1400	1167
G1	2500	2000	1667	500	400	333	2000	1600	1333
G2	2500	2000	1667	500	400	333	2000	1600	1333
Ic1	2250	1800	1500	750	600	500	2000	1600	1333
Sm1	2000	1600	1333	750	600	500	2250	1800	1500
Sm2	2500	2000	1667	500	400	333	2000	1600	1333
CO1	6000	4800	4000	–	–	–	–	–	–
Geothermal Gradient (°C.Km^{-1})	20	25	30	20	25	30	20	25	30

Oliveira et al., 2016; Engelmann de Oliveira and Jelinek, 2017) presented evidence of accelerated Neogene cooling in southeastern Brazil, especially those studying the Brazilian Plateau and those with samples near the margin, where denudation and erosion were active since the opening of the South Atlantic Ocean.

Cenozoic cooling is marked by accelerated exhumation, where samples initiated their final ascent to present-day surface at 85 and 40 Ma (Eocene), comprised by samples Ic1 and Sm1, respectively, and a second group including all other samples, from 30 to 20 Ma (Oligocene) to present. The final cooling episode started for most samples at temperature similar to the AFT PAZ upper limit (~65–55 °C), leading to expectation of cooling between 45 and 35 °C and denudation rates between 15.7 and 87.5 m.Ma^{-1}. The amount of rock section removed since the Eocene to present for the samples that started to cool earlier in this episode is 1333–2000 m (sample Ic1) and 1500–2250 m (sample Sm1). For samples with onset of cooling in the Oligocene, erosion corresponds to 1167–1750 m (sample Cb1) and to 1333–2000 m (all other samples), considering the geothermal gradient of 20, 25 and 30 °C.Km^{-1}, as seen in Tables 2a and 2b The sedimentary record on the southeastern offshore Santos and Espírito Santo basins is compatible with high denudation rates, as many authors found for the margin (*e.g.*, Gallagher et al., 1994, 1995; França et al., 2007; Jelinek et al., 2014; Engelmann de Oliveira et al., 2016). Sedimentary thickness observed in the Espírito Santo basin reaches up to 2500 m (França et al., 2007) and corresponds to deposition from Oligocene to present. The Jequitinhonha basin also has sedimentary thickness up to 2750 m (Rangel et al., 2007), compatible with the estimates on denudation from this study. A state of compression responsible for Paleogene cooling (Cogné et al., 2011) supports the evidence of Cenozoic exhumation presented here, in which relief was available for erosion.

As for the Oligocene, epeirogeny played a role due to rearrangement of the Andean orogen; this mountain range began to rise significantly 30 Ma ago when new plate configurations and orthogonal subduction between the Nazca and South American plates took place. Japsen et al. (2012) argued that more than stresses from the Andes, synchronous uplift phases in NE Brazil and SW Africa had common causes, which suggests far-field effects across the spreading center. At this time, a decline occurred in the Atlantic spreading rate between South American and African plates due to changes in plate motions, configuring a scenario where lateral resistance to plate motion played a role (Torsvik et al., 2009). In this configuration, different actions in plate tectonics were operating, and epeirogeny caused by these aforementioned stresses is the best model to explain Oligocene cooling.

Climatic origin for accentuated erosion rates during the Neogene (Zachos et al., 2001; Spier et al., 2006; Morais Neto et al., 2009) triggered renewed erosion by conversion from tropical to semi-arid climate due to global Neogene cooling. On the other hand, $^{40}Ar/^{39}Ar$ geochronology on weathering profiles constrain weathering rates related to erosion in the QF, whose results mainly attribute slow rates of erosion since the Miocene in order to fully develop thick profiles (Carmo and Vasconcelos, 2004, 2006; Carmo, 2005; Vasconcelos and Carmo, 2018), which contrast with the rates found in this study. These authors obtained 4–8 m.Ma^{-1} as weathering front propagation rates and 2 m.Ma^{-1} as the erosion rate for the last 70 Ma in the QF. Analyses of cosmogenic ^{10}Be isotopes for both QF and SER document slow rates of erosion from 2 to 5 m.Ma^{-1} (Salgado et al., 2006, 2007; Barreto et al., 2013) in quartzite and banded iron formation, whereas in granitic rocks rates are no higher than ~13 m.Ma^{-1} (Salgado et al., 2008).

Our results of geothermal gradients show that from the Upper Devonian to present-day the rock section removal of the basement in the Southern Espinhaço Range and the Quadrilátero Ferrífero province was between ~3300 and 5000 m, pointing to the denudation of 3000–~4700 m previously removed in the Meso- Neoproterozoic. This hypothesis is based on metamorphism of ~450 °C in the central portion of the SER (Schöll and Fogaça, 1979) that indicates an 8000 m thick tectonic pile. Considering the argument of Almeida-Abreu and Renger (2002) that the SER represented a glacier dispersion center at *ca.* 1.1 Ga and that it constituted an orographic entity before the end of the Mesoproterozoic, as a result at least *ca.* 4000 m of rocks were removed after the Espinhaço Orogen and before the Bambuí Group deposition, since carbonatic rocks belonging to the latter are found lying on top of the SER (Almeida-Abreu et al., 2001). The presence of carbonatic rocks indicates that the SER was below the regional base level during parts of the Neoproterozoic.

SER and QF recorded two phases of accelerated exhumation separated by protracted tectonism during the Phanerozoic, in which slow cooling and low denudation rates were interspersed with fast cooling and erosion (Fig. 7). Modeling also presupposes no direct tectonic disturbance due to South Atlantic rifting during the Cretaceous, even though post-rifting processes of alkaline body emplacement were

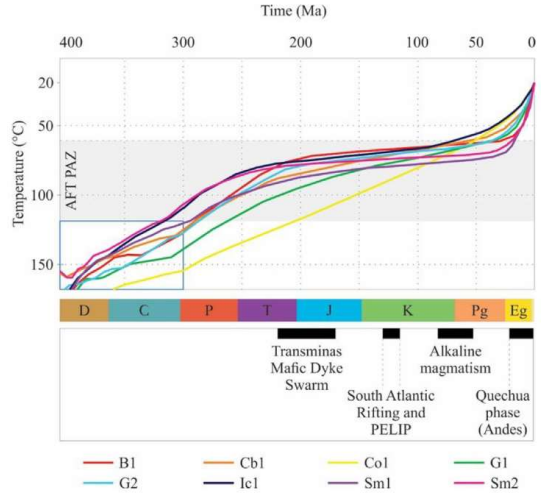

Fig. 7. Thermal history models with the lines indicating the weighted mean path for each sample, derived using software HeFTy (Ketcham, 2005) and associated with regional tectonic events (black rectangles in the bottom), the geologic time scale containing the eras and periods for reference. The light blue box at the bottom left is a t-T box constraint. (For interpretation of the references to colour in this figure legend, the reader is referred to the Web version of this article.)

active. New plate configurations – orthogonal subduction and different spreading rates – between the Nazca, South American and African plates played a role during the Eocene cooling event having epeirogeny as the main mechanism. (U-Th-Sm)/He thermochronological data for zircon as well as zircon fission tracks contribute to elucidate the cooling history of SER and QF, since a larger temperature window would be recorded. Furthermore, such methods may provide additional tools to explore constraints on thermal history and rock provenance for sedimentary units, as well as to understand the amount of rock eroded since the formation of Southern Espinhaço Range units.

6. Conclusions

Combined new and previous AFT thermochronology data constrain the thermotectonic history of Southern Espinhaço Range and Quadrilátero Ferrífero basement, whose AFT apparent ages vary from 187.0 to 91.8 Ma. Events related to continental rifting responsible for the South Atlantic opening, Transminas mafic dyke swarm and the post-rift phases of alkaline rocks emplacement lack correlation with AFT ages. The AFT apparent ages associated with track length distribution and Dpar values allow us to build thermal models and to represent similar cooling history in both areas. The first cooling event started in the Upper Devonian-Early Permian and lasted until the Middle Triassic-Lower Jurassic, bringing the rocks from temperature in excess of 120 °C to the upper limit of the PAZ. This first cooling event is correlated with the Gondwanide orogeny. A slow and protracted cooling phase started in the Middle Triassic-Lower Jurassic until the Eocene-Oligocene. The final cooling event registered fast denudation rates, varying from 15.7 to 87.5 m.Ma^{-1}, and the removal of rock section in the order of 1167–2250 m, considering the geothermal gradients analyzed in this study. The onset of cooling of this last event initiated in the Eocene-Oligocene at temperature similar to the upper limit of the PAZ until present day at surface temperature. Multiple causes of such cooling may be (a) epeirogeny – either because of new configurations in the South Atlantic spreading axis or the Andean orogeny adjusting subduction angles and new plate motion settings; (b) climatic origin with accentuated erosion rates in the Neogene contrast with some studies that suggest slow erosion rates. Epeirogeny is most relevant in this scenario causing propagation of stresses far from the plate boundaries.

Combining the modeled histories of the samples and assuming geothermal gradients of 20, 25 and 30 °C.Km^{-1} for the study area, we provide an overview on how these regions evolved through time regarding thermotectonic parameters. We also contribute to the understanding and quantification of rates of denudation of each cooling episode and estimate the amount of rock section removed since the Upper Devonian, equivalent to *ca.* 3300–5000 m. Besides understanding the history of these particular regions, the recognition that epeirogeny had a fundamental role in the development of the Brazilian hinterland sheds light on the processes that acted upon the SER and QF.

Acknowledgements

The first author thanks Léo Afraneo Hartmann for valuable considerations throughout the writing of this manuscript and Coordenação de Aperfeiçoamento de Pessoal de Nível Superior - CAPES, Brazil, for financial support. A. Jelinek thanks Conselho Nacional de Desenvolvimento Científico e Tecnológico - CNPq (Project 303184/2017-5). The authors are grateful for reviews of Maurício Parra and an anonymous reviewer that led to improvement of the manuscript.

Appendix A. Supplementary data

Supplementary data to this article can be found online at https://doi.org/10.1016/j.jsames.2019.102352.

References

Abreu, A.A., 1982. Análise geomorfológica: reflexão e aplicação. Uma contribuição ao conhecimento das formas de relevo do Planalto de Diamantina-MG. Ph.D. thesis. Univ. São Paulo.

Alexandrino, C.H., Hamza, V.M., 2008. Estimates of heat flow and heat production and a thermal model of the São Francisco craton. Int. J. Earth Sci. 97, 289–306. https://doi.org/10.1007/s00531-007-0291-yAlkmim.

Alkmim, F.F., Marshak, S., 1998. Transamazonian orogeny in the southern São Francisco craton, Minas Gerais, Brazil: evidence for Paleoproterozoic collision and collapse in the Quadrilátero Ferrífero. Precambrian Res. 90, 29–58. https://doi.org/10.1016/S0301-9268(98)00032-1.

Alkmim, F.F., Martins-Neto, M.A., 2012. Proterozoic first-order sedimentary sequences of the São Francisco craton, eastern Brazil. Mar. Pet. Geol. 33, 127–139. https://doi.org/10.1016/j.marpetgeo.2011.08.011.

Almeida, F.F.M., 1977. O Cráton do São Francisco. Rev. Bras. Geociencias 7 (4), 349–364 Online accessed on April 5th, 2019.

Almeida, F.F.M., Carneiro, C.D.R., Mizusaki, A.M.P., 1996. Correlação do magmatismo das Bacias da Margem Continental Brasileira com o das áreas emersas adjacentes. Rev. Bras. Geosci. 23 (3), 125–138 Online Accessed on April 5th, 2019.

Almeida, F.F.M., Hasui, Y., Brito Neves, B.B., Fuck, R.A., 1981. Brazilian structural provinces: an introduction. Earth Sci. Rev. 17, 1–29. https://doi.org/10.1016/0012-8252(81)90003-9.

Almeida-Abreu, P.A., 1995. O Supergrupo Espinhaço da Serra do Espinhaço Meridional (Minas Gerais): o rifte, a bacia e o orógeno. Geonomos 3 (1), 1–18. https://doi.org/10.18285/geonomos.v3i1.211.

Almeida-Abreu, P.A., Queiroz, W.P., Rosière, C.A., Renger, F.E., 2001. A bacia foredeep do Orógeno Espinhaço da Serra do Espinhaço Meridional em Minas Gerais. In: Proceedings of the VIII SNET, Recife, Brazil.

Almeida-Abreu, P.A., Renger, F.E., 2002. Serra do Espinhaço Meridional: Um orógeno de colisão do Mesoproterozoico. Rev. Bras. Geociencias 32, 1–14. https://doi.org/10.25249/0375-7536.20023210114.

Almeida-Abreu, P.A., Renger, F.E., 2007. Stratigraphie und Fazies der südlichen Serra do Espinhaço, Minas Gerais, Brasilien. Zeitschrift der Deutschen Gesellschaft fur Geowissenschaften 158, 9–29. https://doi.org/10.1127/1860-1804/2007/0158-0009.

Augustin, C.H.R.R., Coe, H.H., Chueng, K.F., Gomes, J.G., 2014. Analysis of geomorphic dynamics in ancient quartzite landscape using phytolith and carbon isotopes, Espinhaço Range, Minas Gerais, Brazil. Géomorphologie 20 (4), 355–376 Online accessed on April 4th, 2019.

Barreto, H.N., Varajão, C.A.C., Braucher, R., Bourlès, D.L., Salgado, A.A.R., Varajão, A.F.D.C., 2013. Denudation rates of the southern Espinhaço range, Minas Gerais, Brazil, determined by in situ-produced cosmogenic beryllium-10. Geomorphology 191, 1–13. https://doi.org/10.1016/j.geomorph.2013.01.021.

Brito Neves, B.B., Fuck, R.A., Pimentel, M.M., 2014. The Brasiliano collage in South America: a review. Braz. J. Geol. 44 (3), 493–518. https://doi.org/10.5327/Z2317-4889201400030010.

Burbank, D., Anderson, R.S., 2001. Rates of erosion and uplift. In: Burbank, D., Anderson,

R.S. (Eds.), Tectonic Geomorphology, pp. 287p.
Carmo, I.O., 2005. Geocronologia Do Intemperismo Cenozóico No Sudeste Do Brasil (Weathering Geochronology during the Cenozoic in Southeastern Brazil). Ph.D. thesis. Universidade Federal do Rio de Janeiro.
Carmo, I.O., Vasconcelos, P.M., 2004. Geochronological evidence for pervasive Miocene weathering, Minas Gerais, Brazil. Earth Surf. Process. Landforms 29, 1303–1320. https://doi.org/10.1002/esp.1090.
Carmo, I.O., Vasconcelos, P.M., 2006. $^{40}Ar/^{39}Ar$ geochronology constraint on late Miocene weathering rates in Minas Gerais, Brazil. Earth Planet. Sci. Lett. 241, 80–94. https://doi.org/10.1016/j.epsl.2005.09.056.
Carneiro, M.A., Noce, C.M., Teixeira, W., 1995. Evolução tectônica do Quadrilátero Ferrífero sob o ponto de vista da Geocronologia. Revista da Escola de Minas 48, 264–274.
Chang, H.K., Kowsmann, R.O., Figueiredo, A.M.F., Bender, A.A., 1992. Tectonics and stratigraphy of the East Brazil Rift system: an overview. Tectonophysics 213, 97–138. https://doi.org/10.1016/0040-1951(92)90253-3.
Chaves, A.O., 2013. Enxames de diques máficos de Minas Gerais: O estado da arte. Geonomos 21 (1), 29–33. https://doi.org/10.18285/geonomos.v21i1.253.
Chaves, A.O., Neves, J.M.C., 2005. Radiometric ages, aeromagnetic expression, and general geology of mafic dykes from southeastern Brazil and implications for African-South American correlations. J. South Am. Earth Sci. 19, 387–397. https://doi.org/10.1016/j.jsames.2005.04.005.
Chemale Jr., F., Dussin, I.A., Martins, M., Santos, M.N., 2011. Nova abordagem tectono-estratigráfica do Supergrupo Espinhaço em sua porção meridional (MG). Geonomos 19 (2), 173–179. https://doi.org/10.18285/geonomos.v19i2.52.
Chemale Jr., F., Dussin, I.A., Alkmim, F.F., Martins, M.S., Queiroga, G., Armstrong, R., Santos, M.N., 2012. Unravelling a Proterozoic basin history through detrital zircon geochronology: the case of the Espinhaço Supergroup, Minas Gerais, Brazil. Gondwana Reserach 22, 200–206. https://doi.org/10.1016/j.gr.2011.08.016.
Chemale Jr., F., Quade, H., van Schmus, W.R., 1998. Petrography, geochemistry and geochronology of the Borrachudo and Santa Bárbara metagranites, Quadrilátero Ferrífero, Brazil. Zbl.Geol.Paläont. 3 (6), 739–750.
Cherem, L.F.S., Varajão, C.A.C., Braucher, R., Bourlès, D., Salgado, A.A.R., Varajão, A.F.D.C., 2012. Long-term evolution of denudational escarpments in southeastern Brazil. Geomorphology 173–174, 118–127. https://doi.org/10.1016/j.geomorph.2012.06.002.
Cogné, N., Gallagher, K., Cobbold, P.R., 2011. Post-rift reactivation of the onshore margin of southeast Brazil: evidence from apatite (U–Th)/He and fission-track data. Earth Planet. Sci. Lett. 309 (1), 118–130. https://doi.org/10.1016/j.epsl.2011.06.025.
Cogné, N., Gallagher, K., Cobbold, P.R., Riccomini, C., Gautheron, C., 2012. Post-breakup tectonics in southeast Brazil from thermochronological data and combined inverse-forward thermal history modeling. J. Geophys. Res. 117, B11413. https://doi.org/10.1029/2012JB009340.
D'agrella-Filho, M.S., Pacca, I.G., Teixeira, W., Onstott, T.C., Renne, P.R., 1990. Paleomagnetic evidence for the evolution of Meso- to Neo-Proterozoic rocks in central-eastern Brazil. Palaeogeogr. Palaeoclim. Palaeoec. 80, 255–265. https://doi.org/10.1016/0031-0182(90)90136-U.
Derby, O.A., 2010. The iron ores of Brazil. Rev. Esc. Minas 63 (3), 473–479. https://doi.org/10.1590/S0370-44672010000300008.
De Wit, M., Jeffery, M., Bergh, H., Nicolaysen, L., 1988. Geologic Map of Sectors of Gondwana. AAPG and University of Witwatersrand, Tulsa.
Donelick, R.A., O'Sullivan, P.B., Ketcham, R.A., 2005. Apatite fission-track analysis. In: In: Reiners, P.W., Ehlers, T.A. (Eds.), Low-Temperature Thermochronology: Techniques, Interpretations, and Applications. Reviews in Mineralogy and Geochemistry, vol 58. Mineralogical Society of America, Washington, pp. 49–94.
Dussin, T.M., 1994. Associations volcano-plutoniques de l'Espinhaço Meridional (SE-Bresil). PhD thesis. Univ. D'Orleans, France, pp. 177.
Dussin, I.A., Dussin, T.M., 1995. Supergrupo Espinhaço: Modelo de Evolução Geodinâmica. Geonomos 1, 19–26. https://doi.org/10.18285/geonomos.v3i1.212.
Engelmann de Oliveira, C.H.E., Jelinek, A.R., Chemale, F., Cupertino, J.A., 2016. Thermotectonic history of the southeastern Brazilian margin: evidence from apatite fission track data of the offshore Santos Basin and continental basement. Tectonophysics 685, 21–34. https://doi.org/10.1016/j.tecto.2016.07.012.
Engelmann de Oliveira, C.H., Jelinek, A.R., 2017. História termotectônica da margem continental brasileira a partir de dados de traços de fissão em apatita. Pesquisa em Geociências 44 (3), 387–400. https://doi.org/10.22456/1807-9806.83263.
Eschwege, W.L.v., 1822. Geognostisches Gemälde von Brasilien und wahrscheinliches Muttergestein der Diamanten. Weimar. Landes Industrie Comptoir, pp. 44p.
Farina, F., Albert, C., Martínez Dopico, C., Aguilar Gil, C., Moreira, H., Hippertt, J.P., Cutts, K., Alkmim, F.F., Lana, C., 2016. The Archean-Paleoproterozoic evolution of the Quadrilátero Ferrífero (Brasil): current models and open questions. J. South Am. Earth Sci. 68, 4–21. https://doi.org/10.1016/j.jsames.2015.10.015.
Fernandes, M.L.S., Pedrosa-Soares, A.C., Noce, C.M., Wiedemann, C., Correia-Neves, J.M., 2000. U-Pb geochronology of the Borrachudos suite: evidence of Brasiliano anorogenic granites (Araçuaí belt, Minas Gerais, Brazil). International Geological Congress 31, Rio de Janeiro, Abstracts Volume, CD.
Fonseca, B.M., Augustin, C.H.R.R., 2014. Análise morfométrica de bacias de drenagem e sua relação com a estrutura geológica, serra do Espinhaço Meridional–MG. Revista Brasileira de Geomorfologia 15 (2), 153–172. https://doi.org/10.20502/rbg.v15i2.296.
França, R.L., Del Rey, A.C., Tagliari, C.V., Brandão, J.R., Fontanelli, P.R., 2007. Bacia do Espírito Santo. Bol. Geoc. Petrobras 15 (2), 501–509 Online accessed on March 22nd, 2019.
Fleischer, R.L., Price, P.B., Symes, E.M., Miller, D.S., 1964. Fission-track ages and track-annealing behavior of some micas. Science 143 (3604), 349–351. https://doi.org/10.1126/science.143.3604.349.
Galbraith, R.F., 1981. On statistical models for fission track counts. Math. Geol. 13 (6), 471–478. https://doi.org/10.1007/BF01034498.
Galbraith, R.F., Laslett, G.M., 1993. Statistical models for mixed fission track ages. Nucl. Tracks Radiat. Meas. 21, 459–470. https://doi.org/10.1016/1359-0189(93)90185-C.
Gallagher, K., 1995. Evolving temperature histories from apatite fission-track data. Earth Planet. Sci. Lett. 136, 421–435. https://doi.org/10.1016/0012-821X(95)00197-K.
Gallagher, K., Brown, R., Johnson, C., 1998. Fission track analysis and its applications to geological problems. Annu. Rev. Earth Planet Sci. 26, 519–572. https://doi.org/10.1146/annurev.earth.26.1.519.
Gallagher, K., Hawkesworth, C.J., Mantovani, M.S.M., 1994. The denudation history of the onshore continental margin of SE Brazil inferred from apatite fission track data. J. Geophys. Res. 99, 18117–18145. https://doi.org/10.1029/94JB00661.
Gallagher, K., Hawkesworth, C.J., Mantovani, M.S.M., 1995. Denudation, fission track analysis and the long-term evolution of passive margin topography: application to the southeast Brazilian margin. J. South Am. Earth Sci. 8, 65–77. https://doi.org/10.1016/0895-9811(94)00042-Z.
Gleadow, A.J.W., Duddy, I.R., Green, P.F., Lovering, J.F., 1986. Confined fission track lengths in apatite: a diagnostic tool for thermal history analysis. Contrib. Mineral. Petrol. 94, 405–415. https://doi.org/10.1007/BR00376334.
Green, P.F., 1986. On the thermo-tectonic evolution of Northern England: evidence from fission track analysis. Geol. Mag. 123 (5), 493–506. https://doi.org/10.1017/S0016756800035081.
Harman, R., Gallagher, K., Brown, R., Raza, A., Bizzi, L., 1998. Accelerated denudation and tectonic/geomorphic reactivation of the cratons of northeastern Brazil during the Late Cretaceous. J. Geophys. Res. 103 (B11). https://doi.org/10.1029/98JB02524.
Hartmann, L.A., Endo, I., Suita, M.T.F., Santos, J.O.S., Frantz, J.C., Carneiro, M.A., Naughton, N.J., Barley, M.E., 2006. Provenance and age delimitation of Quadrilátero Ferrífero sandstones based on zircon U–Pb isotopes. J. South Am. Earth Sci. 20, 273–285. https://doi.org/10.1016/j.jsames.2005.07.015.
Hiruma, S.T., Riccomini, C., Modenesi-Gauttieri, M.C., Hackspacher, P.C., Hadler Neto, J.C., Franco-Magalhaes, A.O.B., 2010. Denudation history of the Bocaina Plateau, Serra do Mar, southeastern Brazil: relationships to Gondwana breakup and passive margin development. Gondwana Res. 18, 674–687. https://doi.org/10.1016/j.gr.2010.03.001.
Hurford, A.J., 1990. International union of geological sciences subcomission on geochronology recommendation for the standardization of fission track dating calibration and data reporting. Nucl. Tracks Radiat. 17 (3), 233–236. https://doi.org/10.1016/1359-0189(90)90040-5.
Isotta, C.A.L., Rocha-Campos, A.C., Yoshida, R., 1969. Striated pavement of the upper Precambrian glaciation in Brazil. Nature 222, 466–468. https://doi.org/10.1038/222466a0.
Japsen, P., Bonow, J.M., Green, P.F., Cobbold, P.R., Chiossi, D., Lilletveit, R., Magnavita, L.P., Pedreira, A., 2012. Episodic burial and exhumation in NE Brazil after opening of the South Atlantic. Geol. Soc. Am. Bull. 124, 800–816. https://doi.org/10.1130/B30515.1.
Jelinek, A.R., Chemale Jr., F., van der Beek, P.A., Guadagnin, F., Cupertino, J.A., 2014. Denudation history and landscape evolution of the northern East-Brazilian continental margin from apatite fission-track thermochronology. J. South Am. Earth Sci. 54, 158–181. https://doi.org/10.1016/j.jsames.2014.06.001.
Ketcham, R.A., 2005. Forward and inverse modeling of low-temperature thermochronometry data. Rev. Mineral. Geochem. 58, 275–314. https://doi.org/10.2138/rmg.2005.58.11.
Ketcham, R.A., Carter, A.C., Donelick, R.A., Barbarand, J., Hurford, A.J., 2007. Improved modeling of fission-track annealing in apatite. Am. Mineral. 92, 799–810. https://doi.org/10.2138/am.2007.2281.
Ketcham, R.A., Donelick, R.A., Donelick, M.B., 2000. AFTSolve: a program for multi-kinetic modeling of apatite fission-track data. Geol. Mater. Res. 2, 1–2 Online accessed on April 5th, 2019.
King, L.C., 1956. Geomorfologia do Brasil oriental. Ver. Bras. Geogr. 18 (2), 1–147 Online accessed on October 9th, 2018.
Knauer, L.G., Ebert, H.D., 1997. Estruturação tectônica da região de Diamantina, MG e considerações sobre a idade do Orógeno Espinhaço. VI Simp. Nac. Est. Tectônicos 56–58 Abstract.
Korschinek, G., Bergmaier, A., Faestermann, T., Gerstmann, U.C., Knie, K., Rugel, G., Wallner, A., Dillmann, I., Dollinger, G., Lierse von Gostomski, Ch, Kossert, K., Maiti, M., Poutivtsev, M., Remmert, A., 2010. A new value for the half-life of ^{10}Be by Heavy-Ion Elastic Recoil Detection and liquid scintillation counting. Nucl. Instrum. Methods Phys. Res. Sect. B Beam Interact. Mater. Atoms 268 (2), 187–191. https://doi.org/10.1016/j.nimb.2009.09.020.
Kuchle, J., Scherer, C.M.S., Born, C.C., Alvarenga, R.S., Adegas, F.A., 2011. A contribution to regional stratgraphic correlations of the Afro-Brazilian depression – the Dom João Stage (Brotas Group and equivalent units – late Jurassic) in Northeastern Brazilian sedimentary basins. J. South Am. Earth Sci. 31 (4), 358–371. https://doi.org/10.1016/j.jsames.2011.02.007.
Machado, N., Schrank, A., Abreu, F.R. de, Knauer, L.G., Almeida-Abreu, P.A., 1989. Resultados preliminares da geocronologia U/Pb na Serra do Espinhaço Meridional. In: Simp. Geol. Minas Gerais, 5, SBG, Belo Horizonte, Anais, pp. 171–174 Online accessed in June 5th, 2019.
Machado, N., Noce, C.M., Ladeira, E.A., Belo de Oliveira, O., 1992. U–Pb geochronology of Archean magmatism and Proterozoic metamorphism in the Quadrilátero Ferrífero, southern São Francisco craton, Brazil. Geol. Soc. Am. Bull. 104, 1221–1227. 2. https://doi.org/10.1130/0016-7606(1992)104<1221:UPGOAM>2.3.CO.
Machado, N., Noce, C.M., Feng, R., 1993. Idades Pb 207/Pb206 de zircões detríticos de rochas meta-sedimentares da região do Quadrilátero Ferrífero, sul do Cráton do São Francisco. Considerações sobre as áreas fontes e idades de sedimentação. In: Anais II Simpósio de Geologia do Cráton do São Francisco, Salvador. Soc. Bras. Geol., Nuúcleo

Bahia/Sergipe, pp. 149–151.
Machado, N., Schrank, A., Noce, C.M., Gauthier, G., 1996. Ages of detrital zircon from Archean-Paleoproterozoic sequences Implications for Greenstone Belt setting and evolution of a Transamazonian foreland basin in Quadrilátero Ferrífero, southeast Brazil. Earth Planet. Sci. Lett. 141, 259–276. https://doi.org/10.1016/0012-821X(96)00054-4.
Marshak, S., Alkmim, F.F., 1989. Proterozoic contraction/extension tectonics of the southern SaÄo Francisco region, Minas Gerais, Brazil. Tectonics 8 (3), 555–571. https://doi.org/10.1029/TC008i003p00555.
Marshak, S., Tinkham, D., Alkmim, F.F., Brueckner, H., Bornhorst, T., 1997. Dome-and-keel provinces formed during Paleoproterozoic orogenic collapse – core complexes, diapirs, or neither? Examples from the Quadrilátero Ferrífero and the Penokean orogeny. Geology 25 (5), 415–418. https://doi.org/10.1130/0091-7613(1997)025<0415:DAKPFD>2.3.CO;2.
Morais Neto, J.M., Hegarty, K.A., Karner, G.D., Alkmim, F.F., 2009. Timing and mechanisms for the generation and modification of the anomalous topography of the Borborema Province, northeastern Brazil. Mar. Pet. Geol. 26, 1070–1086. https://doi.org/10.1016/j.marpetgeo.2008.07.002.
Moreira, J.L.P., Esteves, C.A., Rodrigues, J.J.G., Vasconcelos, C.S., 2006. Magmatismo, sedimentação e estratigrafia da porção norte da Bacia de Santos. Bol. Geociênc.Petrobras 14 (1), 161–170 Online accessed on April 5th, 2019.
Mohriak, W.U., Leroy, S., 2012. Architecture of rifted continental margins and break-up evolution: insights from the South Atlantic, Noth Atlntic and red Sea-Gulf of Aden conjugate margins. In: In: Mohriak, W.U., Danfort, A., Post, P.J., Brown, D.E., Tari, G.C., Nemcok, M., Sinha, S.T. (Eds.), Conjugate Divergent Margins, vol. 369 Geol. Soc. London, Spec. Publ. https://doi.org/10.1144/SP369.17.
Noce, C.M., 1995. Geocronologia dos eventos magmáticos, sedimentares e metamórficos na região do Quadrilátero Ferrífero, Minas Gerais. Ph.D. Thesis. University de São Paulo Online accessed on April 5th, 2019.
Noce, C.M., Teixeira, W., Quéméneur, J.J.G., Martins, V.T.S., Bolzachini, E., 2000. Isotopic signatures of Paleoproterozoic granitoids from southern São Francisco craton, NE Brazil, and implications for the evolution of the transamazonian orogeny. J. South Am. Earth Sci. 13, 225–239. https://doi.org/10.1016/S0895-9811(00)00019-5.
Paula-Santos, G.M., Babinski, M., Kuchencecker, M., Caetano-Filho, S., Trindade, R.I., Pedrosa-Soares, A.C., 2015. New evidence of an Ediacaran age for the Bambuí Group in Southern São Francisco craton (Eastern Brazil) from zircon U-Pb data and isotope chemostratigraphy. Gondwana Res. 28 (2), 702–720. https://doi.org/10.1016/j.gr.2014.07.012.
Pedrosa-Soares, A.C., Wiedemann-Leonardos, C.M., 2000. Evolution of the Araçuaí belt and its connection to the ribeira belt, eastern Brazil (Org.) In: In: Cordani, U.G., Milani, E.J., Thomaz Filho, A., Campos, D.A. (Eds.), Tectonic Evolution of South America. 1ed. Rio de Janeiro: IGC Brazil 2000, vol. 2000. pp. 265–285. https://doi.org/10.13140/2.1.3802.5928. Online accessed on June 11th, 2019, on ResearchGate.
Pedrosa-Soares, A.C., Noce, C.M., Wiedemann, C., Pinto, C.P., 2001. The Araçuaí-West-Congo Orogen in Brazil: an overview of a confined orogen formed during Gondwanaland assembly. Precambrian Res. 110 (1–4), 307–323. https://doi.org/10.1016/S0301-9268(01)00174-7. Online accessed on June 11th, 2019, on ResearchGate.
Petri, S., Campanha, V.A., 1981. Brazilian continental cretaceous. Earth Sci. Rev. 17, 69–85. https://doi.org/10.1016/0012-8252(81)90006-4.
Pflug, R., 1965. A Geologia da parte meridional da Serra do Espinhaço e zonas adjacentes. Rio de Janeiro, DNPM/DGM, Boletim, vol. 266. pp. 51.
Potter, P.E., 1997. The Mesozoic and Cenozoic paleodrainage of South America: a natural history. J. South Am. Earth Sci. 10 (5–6), 331–344. https://doi.org/10.1016/S0895-9811(97)00031-X.
Price, P.B., Walker, R.M., 1963. Fossil tracks of charged particles in mica and the age of minerals. J. Geophys. Res. 68, 4847–4862. https://doi.org/10.1029/JZ068i016p04847.
Rangel, H.D., Oliveira, J.L.F., Caixeta, J.M., 2007. Bacia de Jequitinhonha (Jequitinhonha basin). Bol. Geo. Petrobras 15 (2), 475–483 Online accessed on April 5th, 2019.
Rocha-Campos, A.C., Cordani, U.G., Kawashita, K., Sonoki, H.M., Sonoki, I.K., 1988. Age of Parana flood volcanism. In: Piccirillo, E.M., Melfi, A.J. (Eds.), The Mesozoic Flood Volcanism of the Parana Basin: Petrogenetic and Geophysical Aspects. Inst. Astron. Geofis. USP, São Paulo, pp. 25–45.
Saadi, A., 1995. A geomorfologia da Serra do Espinhaço em Minas Gerais e de suas margens. Geonomos 3 (1), 41–63. https://doi.org/10.18285/geonomos.v3i1.215.
Salgado, A.A.R., Braucher, R., Colin, F., Nalini JR, H.A., Varajão, A.F.D.C., Varajão, C.A.C., 2006. Denudation rates of the Quadrilátero Ferrífero (Minas Gerais, Brazil): preliminary results from measurements of solute fluxes in rivers and in situ-produced cosmogenic ^{10}Be. J. Geochem. Explor. 88, 313–317. https://doi.org/10.1016/j.gexplo.2005.08.064.
Salgado, A.A.R., Varajão, C., Colin, F., Braucher, R., Varajão, A., Nalini Jr., H., 2007. Study of the erosion rates in the upper Maracujá Basin (Quadrilátero Ferrífero/MG, Brazil) by the *in situ* produced cosmogenic ^{10}Be method. Earth Surf. Process. Landforms 32, 905–911. https://doi.org/10.1002/esp.1448.
Salgado, A.A.R., Braucher, R., Colin, F., Varajão, A.F.D., Nalini Júnior, H.A., 2008. Relief evolution of the Quadrilátero Ferrífero (Minas Gerais, Brazil) by means of (^{10}Be) cosmogenic nuclei. Z. Geomorphol. 52, 317–323. https://doi.org/10.1127/0372-8854/2008/0052-0317.
Schannor, M., 2018. Geodynamic and Metamorphic Evolution of the Araçuaí Orogen (SE Brazil). PhD thesis. Dep. Geologia. Universidade Federal de Ouro Preto Online accessed on November 27th, 2018.
Schöll, W.U., Fogaça, A.C.C., 1979. Mapa geológico da Quadrícula de Guinda, escala 1:25.000. Proj. Map. Geol. Espinhaço Meridional. Dep. Nac. Prod. Min./Centro Geol. Eschwege, Diamantina.
Sgarbi, G.N.C., Sgarbi, P.B.A., Campos, J.E.G., Dardenne, M.A., Penha, U.C., 2001. Bacia Sanfranciscana: O registro Fanerozoico da Bacia do São Francisco. In: Pinto, C.P., Martins-Neto, M.A. (Eds.), Bacia do São Francisco: Geologia e Recursos Naturais. Soc. Bras. Geol. (SBG) – Núcleo MG, Belo Horizonte.
Siga Jr., O., Cordani, U.G., Kawashita, K., Basei, M.A.S., Taylor, P.N., 1987. Aplicação dos isótopos de Sr e Pb nas rochas gnássico-mimatíticas de Itacambira-Barrocão. Anais 4º Simpósio de Geologia de Minas Gerais 45–57.
Spier, C.A., Vasconcelos, M., Oliveira, S.M.B., 2006. ^{40}Ar/^{39}Ar geochronological constraints on the evolution of lateritic iron deposits in the Quadrilátero Ferrífero, Minas Gerais, Brazil. Chem. Geol. 234, 79–104. https://doi.org/10.1016/j.chemgeo.2006.04.006.
Teixeira, W., Sabaté, P., Barbosa, J., Noce, C.M., Carneiro, M.A., 2000. Archean and Paleoproterzoic tectonic evolution of the São Francisco craton, Brazil. In: Cordani, U.G., Milani, E.J., Thomaz Fo, A., Campos, D.A. (Eds.), Tectonic Evolution of South América. Rio de Janeiro, 31st International Geological Congress, Rio de Janeiro, pp. 101–137.
Torsvik, T.H., Rousse, S., Labails, C., Smethurst, M.A., 2009. A new scheme for the opening of the South Atlantic Ocean and the dissection of an Aptian salt basin. Geophys. J. Int. 177, 1315–1333. https://doi.org/10.1111/j.1365-246X.2009.04137.x.
Trompette, R., 1994. Geology of western Gondwana (2000–500 Ma). In: Pan-African/Brasiliano Aggregation of South America and Africa. A.A. Balkema, Rotterdam, pp. 350.
Trompette, R., Uhlein, A., Egydio-da-Silva, M., Karmann, I., 1992. The Brasiliano São Francisco craton revisited (Central Brazil). J. South Am. Earth Sci. 6 (1/2), 49–57. https://doi.org/10.1016/0895-9811(92)90016-R.
Trouw, R.A.J., De Wit, M.J., 1999. Relation between the Gondwanide Orogeny and contemporaneous intracratonic deformation. J. Afr. Earth Sci. 28 (1), 203–213. https://doi.org/10.1016/S0899-5362(99)00024-X.
Uhlein, A., Trompette, R.R., Egydio-Silva, M., 1986. Estruturação tectônica do Supergrupo Espinhaço na região de Diamantina (MG). Rev. Bras. Geociencias 16 (2), 212–216 Online accessed on June 11th, 2019.
Uhlein, A., Trompette, R.R., Egydio-Silva, M., 1998. Proterozoic rifting and closure, SE border of the São Francisco Craton, Brazil. J. South Am. Earth Sci. 11, 191–203. https://doi.org/10.1016/S0895-9811(98)00010-8.
Van Ranst, G., De Grave, J., Pedrosa-Soares, A.C., Tack, L., Baudet, D., Novo, T., 2017. Reactivation of inherited structures during the opening of the South Atlantic: a low-temperature thermochronology study on the Araçuaí orogenic belt (east Brazilian margin). Geophys. Res. Abstr. EGU Gen. Assemb. 2017 Online accessed in December 10th, 2018.
Vasconcelos, P.M., Carmo, I.O., 2018. Calibrating denudation chronology through 40Ar/39Ar weathering geochronology. Earth Sci. Rev. 179, 411–435. https://doi.org/10.1016/j.earscirev.2018.01.003.
Vasconcelos, P.M., Brimhall, G.H., Becker, T.A., Renne, P.R., 1994. 40Ar/39Ar analysis of supergene jarosite and alunite: implications to the paleoweathering history of the western USA and West Africa. Geochem. Cosmochim. Acta 58 (1), 401–420. https://doi.org/10.1016/0016-7037(94)90473-1.
Vermeesch, P., 2009. Radial Plotter: a Java application for fission track, luminescence and other radial plots. Radiat. Meas. 44, 409–410. https://doi.org/10.1016/j.radmeas.2009.05.003.
Zachos, J., Pagani, M., Sloan, L., Thomas, E., Billups, K., 2001. Trends, rhythms, and aberrations in global climate 65 Ma to present. Science 292, 686–693. https://doi.org/10.1126/science.1059412.